View metadata, citation and similar papers at core.ac.uk
brought to you by CORE
provided by DSpace@MIT

1 The motion of kelp blades and the surface renewal model

2

3 Ivy Huang, Jeffrey Rominger and Heidi Nepf *

4 Massachusetts Institute of Technology, Cambridge, Massachusetts

5

6 * Corresponding author: hmnepf@mit.edu

7 Running head: Blade motion and boundary layer renewal

8

Acknowledgments –

We thank Clint Nelson at University of California at Santa Barbara and Kristy Kull at Friday Harbor Labs for supplying *Macrocystis pyrifera* and *Nereocystis luetkeana* blades, respectively; Paul Dobbins, President of Ocean Approved, for his insight regarding kelp morphology and for supplying blades of *Laminaria saccharina*. We also thank the three anonymous reviewers who provided insightful comments that greatly improved this manuscript. This material is based upon work supported by grant number 0751358 from the National Science Foundation Ocean Sciences Division. Ivy Huang was supported by the Massachusetts Institute of Technology Class of 1973 Fund. Connie Lu assisted with preliminary experiments with support from the Massachusetts Institute of Technology Class of 1995 Fund.

Abstract-

We consider how the flapping of kelp blades may enhance the flux of nutrients to a blade, by stripping away the diffusive sub-layer and renewing the fluid at the blade surface. The surface renewal model explains the degree of flux enhancement observed in previous studies under different flow and flapping conditions. We measured the motion of real kelp blades of *Laminaria saccharina*, *Macrocystis pyrifera*, and *Nereocystis luetkeana* under uni-directional current in a laboratory flume. Observed flapping frequencies coupled with the renewal model, suggest that the flapping of blades in the field has the potential to significantly enhance flux to the blade surface at low current speed, but has little affect on flux at high current speeds.

INTRODUCTION

Many species of kelp have blades with a flat morphology in regions of high wave and current action, called exposed sites, and blades with a ruffled morphology in regions of low wave and current action, called sheltered sites (Koehl et al. 2008). Researchers have suggested that this morphological shift between exposed and sheltered sites is a trade-off between the need to minimize drag and prevent breakage and the need to maximize photosynthesis (Gerard and Mann 1979; Koehl and Alberte 1988; Haring and Carpenter 2007). Under steady current ruffled blades spread out and flap, tendencies that increase both light interception and drag (Koehl et al. 2008). Blade flapping has also been observed to enhance the rate of nutrient uptake (Koehl and Alberte 1988). In contrast, flat blades collapse into streamlined clumps under high flow, which reduces drag but also light interception (Koehl et al. 2008). Finally, previous research has suggested that at sheltered sites the flux of nutrients to a blade surface is limited by mass-transport to the blade surface (Gerard and Mann 1979; Wheeler 1980; Koch 1993).

To summarize the above ideas, at exposed sites, the mean and wave-induced flow is consistently high enough that mass-flux limitation does not occur, so that drag reduction dominates the morphological choice, and a streamline blade shape is produced. At sheltered sites, the mean currents are low enough that mass-transfer limitation is a greater threat than hydrodynamic drag, and a ruffled blade shape is produced, because this morphology promotes flapping, and flapping has been observed to enhance flux. In this paper we provide some new insight into this hypothesis by 1) demonstrating that the surface renewal model can explain previous observations of flux to flapping blades, 2) measuring the flapping frequencies of four different real blades, and 3) using the surface renewal model to describe the magnitude of flux enhancement expected from the observed range of flapping frequencies.

How flapping enhances fluxes – the surface renewal model

Previously, the mass-flux to blade surfaces has been described using the thin-film model, which assumes that a static boundary layer exists on the surface of the blade (Wheeler 1980; Hurd et al. 1996). However, some authors have suggested that turbulence and wave-induced blade motion can periodically disturb or strip away the diffusive sub-layer and thereby enhance flux to the blade (Koch 1994; Hurd 2000; Stevens and Hurd 1997). Stevens and Hurd (1997) used the surface renewal model from Higbie (1935) to describe a mechanism of flux enhancement for kelp blades. The model proposes that the flux at a surface is enhanced by the periodic renewal of water at the surface. Each renewal, or disturbance, replaces the fluid in the diffusive sub-layer with fluid from outside this sub-layer, producing an instantaneously higher concentration gradient at the surface and thus higher flux. The subsequent evolution of the concentration profile is described below and depicted in Fig. 1.

Let the surface of the blade be $z = 0$, and z is positive upward. Next to the boundary there exists a fluid region, called the diffusive sub-layer, in which turbulent transport is negligible, and flux occurs only through molecular diffusion. Advection is very small within this layer, and can be neglected. The thickness of the diffusive sub-layer, δ_D, is related to the viscous sub-layer thickness, δ_ν. For fully turbulent boundary layers $\delta_\nu \approx 10\nu/u_*$, with ν the molecular kinematic viscosity and u_* the friction velocity. Because of the difference in magnitude between molecular diffusivity (D) and kinematic viscosity, the diffusive sub-layer is smaller than the viscous sub-layer. Specifically, $\delta_D = \delta_\nu Sc^{-1/3}$, with Schmidt number $Sc = \nu/D$ (Boudreau and Jorgensen 2001). In water $\nu = 10^{-6}$ m^2 s^{-1}, and for most dissolved species $D \approx 10^{-9}$ m^2 s^{-1}, so that in water, we generally find $\delta_D = 0.1\delta_\nu$.

The diffusive sub-layer can control the uptake of nutrients by a blade, if the rate of diffusion across δ_D is slower than the rate of biological incorporation occurring at the surface. Under these conditions we can assume that the blade instantly takes up any chemical arriving at its surface, so that the concentration at the surface is zero, $C(z = 0) = 0$. The concentration at the top of the diffusive sub-layer is C_o. The steady-state concentration profile within the diffusive sub-layer is linear, and the flux is

$$J_s = DC_o/\delta_D \quad (1)$$

The viscous and diffusive sub-layers may be disrupted by wave-action, blade motion, or the passage of vigorous turbulent structures. Any of these events might cause the boundary layer to be stripped away, so that the velocity and concentration just above the surface ($z = 0^+$) are instantaneously reset to the values outside the boundary layers, U and C_o, respectively. Over time both the velocity and concentration gradients are re-established. The time-scale to re-establish the viscous sub-layer, $T_\nu = \delta_\nu^2/\nu$, is much shorter than the time-scale to re-establish the diffusive sub-layer, $T_D = \delta_D^2/D$, because the molecular diffusion of momentum is much faster than the molecular diffusion of most scalars. Specifically, in water ν/D is O(1000) and δ_D/δ_ν is O(0.1), so that T_D/T_ν is O(10). Therefore, it is reasonable to assume that the viscous sub-layer is instantly re-established and to focus on the development of the concentration profile.

Assume that the disturbance re-sets the concentration to a uniform distribution $C(z, t = 0) = C_o$, but that the boundary remains a perfect sink, $C(z = 0) = 0$. The concentration profile then evolves as a function of time and vertical position as shown in Fig. 1, and described by Carslaw and Jaeger (1959) and Stevens and Hurd (1997).

98
$$C(z,t) = \frac{C_o}{\delta_D} z + \frac{2C_o}{\pi} \sum_{n=1}^{\infty} \frac{\cos(n\pi)}{n} \sin\left(\frac{n\pi z}{\delta_D}\right) \exp\left(-\frac{Dn^2\pi^2 t}{{\delta_D}^2}\right) + 2C_o \sum_{n=1}^{\infty} \sin\left(\frac{n\pi z}{\delta_D}\right) \exp\left(-\frac{Dn^2\pi^2 t}{{\delta_D}^2}\right) \left(\frac{1-\cos(n\pi)}{n\pi}\right) \quad (2)$$

99 The gradient of concentration at the blade surface, $\partial C/\partial z|_{z=0}$, is maximum directly after
100 the disturbance and decreases over time until a steady sub-layer is re-established at $t = T_D = \delta_D^2/D$ (Fig. 1). The steady concentration profile is linear, which yields the static sub-layer flux
101 given in Eq. 1. The instantaneous flux is $J = D\partial C/\partial z|_{z=0}$, so that the instantaneous flux is also
102 maximum directly after the disturbance and progressively decreases until reaching the static sub-
103 layer flux given by Eq. 1.

104 If disturbances occur frequently enough, the mean flux to the blade can be enhanced
105 relative to the static sub-layer flux. This is illustrated in Fig. 2, which compares the
106 instantaneous flux (J) and mean flux ($\bar{J}$) for two disturbance regimes. The mean flow is the
107 same for both conditions, producing the same static diffusive sub-layer thickness (δ_D). Each
108 time the sub-layer is disturbed, it requires time $T_D = \delta_D^2/D$ for the instantaneous flux (J) to return
109 to the steady flux (J_s). In case 1 (thick line) the boundary layer is disturbed with a recurrence
110 period of T_1. Because $T_1 > T_D$, the instantaneous flux is equal to the static flux ($J = J_s$) for a
111 significant fraction of time, and the periodic disturbance has only a small influence on the time-
112 averaged flux, $\bar{J}$. That is, $\bar{J}$ is only slightly larger than J_s, as shown in Fig. 2. If the time-
113 interval between disturbances increased further, the mean flux would decrease, approaching J_s.
114 In contrast, in case 2 the disturbance time-scale is shorter than the diffusive time-scale ($T_2 < T_D$),
115 and the time-averaged flux is enhanced relative to the steady-state flux, i.e., $\bar{J} > J_s$ (Fig. 2).

116 We can formalize the progression between the two cases shown in Fig. 2 by comparing
117 the time-averaged flux to the static sub-layer flux over a range of disturbance periods. The time-

averaged flux is estimated by integrating the instantaneous flux, $J = D\partial C/\partial z|_{z=0}$, over the time interval T, as described in Stevens and Hurd (1997),

$$\bar{J} = \frac{DC_o}{\delta_D} + 2\frac{C_o\delta_D}{T}\sum_{n=1}^{\infty}\frac{1}{n^2\pi^2}\left(1-\exp\left(-n^2\pi^2\frac{DT}{{\delta_D}^2}\right)\right) \quad (3)$$

The first term on the right-hand side is the static sub-layer flux (J_s), and the second term is the enhancement associated with the periodic disturbance. By considering the non-dimensional form of Eq. 3, we see that the ratio of disturbance period to diffusion time-scale, T/T_D, controls the degree of flux enhancement.

$$\frac{\bar{J}}{J_s} = 1 + 2\frac{T_D}{T}\sum_{n=1}^{\infty}\frac{1}{n^2\pi^2}\left(1-exp\left(-n^2\pi^2\frac{T}{T_D}\right)\right) \quad (4)$$

If $T/T_D > 6$, the time-average flux is within 5% of the static sub-layer flux, indicating that the periodic disturbance of the boundary layer provides no benefit (Fig. 3). If $T/T_D < 6$, the periodic disturbance enhances the time-averaged flux, e.g., by 30% for $T/T_D = 1$, and by 10-fold for $T/T_D = 0.01$. For $T/T_D < 0.5$, the mean flux given by Eq. 3 converges to within 5% to a function that depends only on the renewal period (T), and diffusion coefficient, D,

$$\bar{J} = 2C_o\sqrt{\frac{D}{\pi T}} \quad (5)$$

This expression was derived by Higbie (1935) to describe heat flux at a solid boundary driven by

140 vigorous turbulence, with the time-scale of disturbance (T), set by the time-scale of turbulent
141 sweeps. Here, we propose that the time-scale of disturbance is set by the frequency of blade
142 flapping. Equation 5, normalized by J_s, is shown by a thin black line in Fig. 3.
143
144 *Observations supporting the surface renewal model*
145 Denny and Roberson (2002) measured heat flux along the surfaces of two copper blade
146 models based on the morphology of the kelp *Eisenia arborea*. The models were mounted in a
147 wind tunnel and oscillated over ±20 degrees at prescribed frequencies (f), between 0.1 and 0.6
148 Hz. The mean flow speed in the tunnel was adjusted to represent conditions in a sheltered (low
149 speed) and an exposed (high speed) field environment. Because the experiments were conducted
150 in air, the experimental velocities were chosen to achieve comparable Reynolds' number
151 between wind tunnel and ocean conditions. The conditions and flux measurements are
152 summarized in Table 1. In contrast to water, in air $Sc = 0.79$. As a result, δ_D and δ_v are very
153 close in scale. The heat flux measurements for the low-speed and high-speed conditions are
154 taken from fig. 4 and fig. 5, respectively, in Denny and Roberson (2002). The flux enhancement
155 is the ratio of flux observed with flapping to that observed without flapping. Under the low-
156 speed flow condition the flux enhancement was as high as 2.9. However, under the high-speed
157 flow condition the flux enhancement ratio was close to one for all cases, i.e., there was no flux
158 enhancement associated with the flapping. The difference in flux enhancement observed in the
159 low and high-speed flow is consistent with the surface renewal model (Fig. 3). Denny and
160 Roberson (2002) do not report the friction velocity, but it can be estimated from the mean
161 velocity U. The best fit was achieved using $u_* = 0.07U$, which is physically reasonable. This
162 value is used in the calculations shown in Table 1. For the low flow condition the disturbance

period, T, is comparable to the diffusion time-scale, specifically T/T_D = 0.45 to 2 (Table 1). According to Eq. 4, flux enhancement should occur for this range of time-scale ratios, and the magnitude of observed flux enhancement (Table 1) is consistent with the renewal model (Fig. 3). In contrast, for the high-flow condition, the diffusion time-scale is significantly shorter (T_D = 0.035 s), because the higher friction velocity leads to a thinner sub-layer. The time-scale ratio (T/T_D) falls between 20 and 110. According to Eq. 4, these disturbance periods should not enhance the flux. The observed fluxes are consistent with this prediction (Table 1, Fig. 3). It is interesting to note that the exposed (triangle) and the sheltered (circle) morphology experienced the same flux enhancement. That is, the frequency, rather than the morphology, was the dominant factor in determining the degree of flux enhancement. This makes sense, because the model blades were stiff (molded copper) and forced to flap at identical frequencies and amplitudes. In the field, however, blade morphology has been observed to influence the flapping amplitude, specifically ruffled blades were observed to have more pronounced flapping than flat blades (Koehl and Alberte 1988). As discussed below, this may be related to a resonant response between the blade's natural frequency and vortex shedding associated with individual ruffles.

Koehl and Alberte (1988) reported enhanced nutrient uptake by real blades of *Nereocystis luetkeana* that were mechanically flapped, relative to blades held stationary in a flume with current. Flapping at 1 to 3 Hz produced flux enhancement of 2.0 and 1.6, for speeds of 0.43 and 0.85 cm s^{-1}, respectively (Table 2). However, the channel flow was laminar. Specifically, for the reported tank cross-section (9 cm^2) and maximum flow speed (0.85 cms^{-1}), the channel Reynolds number would be at most Re = (3 cm)(0.85 cm s^{-1})/(0.01 cm^2 s^{-1}) = 255, which is far below the transition to turbulence, $Re \approx 2000$ (Street and Wylie 1985). Because the flow was laminar, there is no distinct viscous and diffusive sub-layer, and Koehl and Alberte's data cannot

be compared directly to the surface renewal model. However, we can make a qualitative comparison, by letting the duration of the experiment represent the diffusive time-scale T_D in our model. This roughly approximates the fact that the concentration boundary grows continuously through the experiment, i.e., the static condition is not reached within the duration of the measurement. Then, $T/T_D = O(10^{-4})$. Rather than stretch the plot, we placed the Koehl and Alberte (1988) data at $T/T_D = 0.001$ (solid squares), which is reasonable for a qualitative discussion, because the main point is that the observed flux enhancement is far below what would be expected from surface renewal. There are two possible explanations. It is possible that the blades were not mass-transfer limited, i.e., the flux was set by the rate of biological uptake. Or, it is possible that the flapping imposed by Koehl and Alberte (1998) did not completely strip the diffusive sub-layer. Koehl and Alberte (1988) imposed a flapping-amplitude of only 2 cm. In contrast, the blades used by Denny and Roberson (2002) were flapped with the amplitude of 4 cm. The more vigorous flapping imposed by Denny and Roberson (2002) may strip the diffusive sub-layer more completely than the milder flapping used by Koehl and Alberte (1988). Real blades have been observed to flap with amplitudes up to 12 cm (Koehl and Alberte 1988), so greater flux enhancement may be possible in the field. Finally, we note that the Denny and Roberson (2002) experiments were idealized measurements that used heat flux as a proxy for CO_2 uptake. Koehl and Alberte (1988) used real kelp blades and measured actual photosynthesis rates, so that their measurements were likely to be noisier.

Denny and Roberson (2002) attribute the flapping of blades in the field to the interaction between blades and waves. Similarly, Stevens and Hurd (1997) and Stevens et al. (2003) attribute the stripping of the boundary layers to wave orbital motions. These mechanisms are surely at work, but are probably of less importance in a sheltered environment, where waves, as

well as currents, are diminished. Koehl and Alberte (1988) observed blade flapping in the absence of waves in mean currents as low at 6 cm s^{-1}. Similarly, Hurd and Stevens (1997) noted blade motion in flow as low as 0.5 cm s^{-1}. Previous observations also suggest that the ruffles on a blade enhance the amplitude of flapping in uni-directional current. Specifically, ruffled blades of *Nereocystis luetkeana* flapped with amplitudes that were up to six times larger than those observed with flat blades (fig. 5 in Koehl and Alberte 1988).

The ruffled morphology may promote blade flapping by generating unsteady vortices behind the individual ruffles, i.e., similar to the vortex shedding observed behind a circular cylinder (Fig. 4). The vortex shedding is associated with pressure oscillations that may initiate flapping, or even interact with flapping in a resonant fashion. The ruffled blade morphology is similar to a corrugated plate. Flow over a corrugated plate generates vortices that are unsteady at specific frequencies, described by the Strouhal number,

$$St = f_s \, d / U = f_s \, \lambda / 2U \qquad (6)$$

(Blevins 1990, p. 47-53). Here, f_s is the vortex shedding frequency in Hz, and d is the width of a single corrugation (ruffle), or ½ the corrugation (ruffle) wavelength, λ. Using plastic models based on the kelp *Nereocystis luetkeana* (Fig. 4b), the presence of unsteady vortices behind individual ruffles was observed in velocity spectrum measured near the blade surface at flow speeds between 1 and 15 cm s^{-1} (I. Huang unpublished data). The measured Strouhal number, St = 0.25±0.10, was consistent with that reported for corrugated plates (St = 0.19, Blevines 1998). Similarly, Hurd and Stevens (1997) observed flow separation behind individual undulations along a *Macrocystis integrifolia* blade at flow speeds as low at 0.5 cms^{-1}.

232 METHODS

233 Three different species of kelp were obtained from Maine, California, and Washington,
234 through commercial farmers and marine research laboratories. Ruffled *L. saccharina* blades
235 were collected off Little Chebeague Island (43°42'32.77"N, 70°09'06.53"W) in Casco Bay,
236 Maine, on 23 June 2010. These blades were stored in seawater and kept overnight at ~3^{o}C in
237 two 20-liter plastic buckets before being transported to Massachusetts Institute of Technology.
238 Flat *M. pyrifera* blades were collected from Mohawk Reef (34°23'38.7"N, 119°43'44.8"W) in
239 Santa Barbara, California, on 13 July 2010. These blades were picked by hand and shipped the
240 same day in Ziploc bags with paper towels moistened with seawater and surrounded with ice
241 packs. Both ruffled and flat *N. luetkeana* blades were collected between Shady Cove and Point
242 Caution (48°33'3.42" N, 123°0'19.51" W) in Friday Harbor, Washington, on 21 July 2010.
243 These blades were kept overnight in a flow-through seawater tank. Blades from all three sites
244 arrived at the laboratory within 48 hours of collection, and all observations of blade motion were
245 made on the day of arrival. Between measurements, individual blades were kept in a plastic
246 flume (2.74 x 0.22 x 0.20 m) filled with saltwater (PETCO® premium marine salt mix) and
247 amended with sodium nitrate and sodium phosphate, roughly 20x more concentrated than the
248 nutrient levels reported by the World Ocean Atlas (Garcia et al. 2010). Peristaltic pumps
249 continuously re-circulated the water. Ice was added to keep the water cool.

250 Measurements of length, width, and thickness were made for each blade (Table 2).
251 Distinctive features were also recorded. For example, the *L. saccharina* blades had both ruffles
252 and winkles (parallel dimples lining the rib of the blade). The flat *M. pyrifera* blades had
253 longitudinal corrugations and small spikes along the edges.

Individual blades were mounted in a re-circulating glass flume (30.48 x 0.76 x 0.88 m) with a water depth of 0.35 m. The flume's pump speed was set incrementally, between 30 and 60 Hz, by a PowerFlex40 drive pump (Allen-Bradley), and the water velocity was measured using an acoustic Doppler velocimeter (Nortek Vectrino) with a downward-looking probe. The tip of the velocity probe was positioned at mid-width and approximately mid-depth, measuring velocities 0.17 m above the bottom of the flume. Each blade was suspended 0.14 m above the glass bottom using fishing line strung between a weight on the flume bed and a crossbar spanning the top of the flume. After each flow adjustment, we waited a minimum of five minutes to allow the flow and the blade motion to adjust to a steady condition before any measurements were recorded. The flat blades of *N. luetkeana* were too long to deploy in the flume test section and were cut. As a result, the length of the flat *N. luetkeana* blades is not representative of mature blades found in nature.

The vertical motion of each blade was recorded using a high-resolution digital camera (Sony model number DFW-X710). A 1.25 cm by 1.25 cm black and white grid was placed behind the opposite flume wall to provide a reference scale for the blade motion. The resolution of each measurement was set by the pixel size, which corresponded to 0.5 mm. Two 100 W portable lamps were used to increase the light contrast between the blade and its background. Preliminary observations suggested that the dominant frequency of blade motion was close to 0.5 Hz. In order to capture a statistically representative number of cycles, we initially chose a record length of about 60 s (30 cycles). A total of 1000 frames were collected for each *L. saccharina* and *M. pyrifera* blade, at 15 frames per second. The number of frames was increased to 3000 (200 s) for each ruffled and flat *N. luetkeana* blade, to better resolve lower frequency motions.

Except for *L. saccharina*, which was measured at a constant velocity, the *M. pyrifera* and *N. luetkeana* blades were measured at four different velocities between 0.15 and 0.32 m s^{-1}.

The raw images were converted to black and white files, isolating a black blade against a white background. A Matlab® script was written to locate the top of the blade at each longitudinal position within each image. To identify the peak frequencies of blade motion, the time-varying position of the blade tip was passed through a Fast Fourier Transform (FFT) function with a five point smoothing window. The range of blade motion was defined as the difference between the maximum and minimum blade tip positions. The amplitude of blade motion was defined as half the range. Due to the length of the *N. luetkeana* blades, the camera was only able to capture the motion of the downstream half of the blade.

RESULTS

The geometric measurements of each blade are summarized in Table 2. Fig. 5 provides an example of the blade motion analysis. Under a current of 22 cm s^{-1}, the tip of a *M. pyrifera* blade oscillated over a range of ±1.6 cm (Fig. 5a). Spectral analysis of the tip motion revealed peaks at 0.10, 0.19, and 0.41 Hz. At least two distinct modes are suggested by the instantaneous traces of the blade position, examples of which are shown in Fig. 5b.

Fig. 6a presents the lowest (open symbols) and the highest (solid symbols) of the frequency peaks extracted from the blade tip motion. The vertical bars represent the standard deviation among the blades within a given species and morphology. The lowest frequency peaks occur between 0.05 and 0.1 Hz, corresponding to 10 to 20 s periods. The highest frequency peaks are around 0.5 Hz, corresponding to a 2 s period. In most cases the frequency does not show a significant correlation with velocity. The one exception is *M. pyrifera*, for which the

299 lowest frequency increases slightly with increasing velocity (Fig. 6a, open triangle). Koehl and
300 Alberte (1988) also observed the flapping of flat and ruffled *N. leutkeana* blades. The frequency
301 was not reported in that paper, but M. Koehl (pers. com.) confirmed that the frequencies used for
302 mechanical flapping were the same as those observed with freely flapping blades, i.e., one to
303 three Hz, with lower frequencies associated with the ruffled blades. This range is consistent with
304 the 0.5 Hz peaks observed in this study.
305 The amplitude of blade motion normalized by blade length is shown in Fig. 6b. The
306 vertical bars represent the standard deviation among the blades within a given species and
307 morphology. The ruffled blade of *L. saccharina* produced motion with notably higher relative
308 amplitude (0.12) that was comparable to the peak amplitudes observed by Koehl and Albere
309 (1988). However, the ruffled and flat blades of *N. leutkeana* have comparable values of relative
310 amplitude. Considering the variation within the species and morphological sub-groups
311 (represented by the vertical bar), the amplitude has no dependence on velocity. These results
312 stand in contrast to previous observations, which are included in Fig. 6b for comparison. Koehl
313 and Alberte (1988) measured higher amplitudes for ruffled blades than for flat blades of *N.*
314 *leutkeana*. In addition, they noted a strong dependence on velocity for the ruffled blades,
315 observing a maximum amplitude at 0.3 m s^{-1}, and lower amplitudes at higher and lower velocity.
316

317 DISCUSSION

318 Based on the measured ruffle and winkle dimensions (Table 2) and the previously
319 measured Strouhal number, $St = 0.25$, we expect unsteady vortex shedding to occur at
320 frequencies between 2 and 8 Hz, and to be dependent on the flow speed (Eq. 6). However, the
321 observed frequencies of blade motion are lower than this and are largely uncorrelated to velocity.

This suggests that the observed frequencies are not set by the vortex shedding, but represent a natural frequency of the blades. However, the vortex shedding may still provide the forcing for the flapping. At some velocities the forced and natural frequencies may be in resonance, which would likely produce much higher amplitudes of motion. Such a resonance may explain Koehl and Alberte's (1988) observation of a much higher flapping amplitude at $U = 30$ cm s^{-1} for ruffled blades (Fig. 6b). An undulation wavelength was not reported in Koehl and Alberte (1988), but we can work in reverse to estimate the wavelength needed to produce resonance at about 1 Hz. From Eq. 6, $\lambda = 15$ cm. This undulation wavelength is consistent with values estimated from images of *N. luetkeana* included in Koehl 2008, $\lambda = 10 \pm 3$ cm, suggesting that the enhanced amplitude observed by Koehl and Alberte (1988) at $U = 30$ cm s^{-1} was due to a resonance between the natural frequency of the blades and the shedding frequency of undulations. We can also estimate the velocity at which resonance might occur for the blades used in the current study. Using a typical undulation wavelength, $\lambda = 4$ cm (Table 3), and setting $f_s = 0.05$ to 0.5 Hz (the observed frequencies), Eq. 6 suggests that velocity in the range $U = 0.4$ to 4 cm s^{-1} would produce resonance. Unfortunately, we were unable to consider such low velocities with the available flume, so that we could not examine whether resonance occurred. However, it is interesting to note that resonance would occur at velocities typical of sheltered environments.

Over the limited range of velocity that could be tested in this study, the blade frequencies were not dependent on flow speed. With caution, we will assume that the observed frequencies are representative of a wider range of flow speeds in the field. We can then use the renewal model to examine whether the observed frequencies have the potential to enhance nutrient flux under field conditions (Fig. 7). For a given flow speed, U, the diffusion time scale, $T_D = \delta_D^2/D$, is

345 set by the relations discussed above, i.e., $u_* = 0.07U$, $\delta_\nu = 10\nu u_*^{-1}$, and $\delta_D = 0.1\delta_\nu$, and using a
346 representative diffusivity of nutrients in water, $D = 10^{-9}$ m^2 s^{-1}. For a fixed ratio $T/T_D = A$, we can
347 write $T = AT_D = A\nu D^{-1}(0.07U)^{-2}$, such that T vs. U corresponds to a line in log-log space. Four
348 such lines are shown in Fig. 7, corresponding to $T/T_D = 0.01$, 0.1, 1 and 6. According to Eq. 4,
349 these lines represent the following flux enhancement: $\bar{J}/J_s = 10$ ($T/T_D = 0.01$), $\bar{J}/J_s = 3.5$ (T/T_D
350 $= 0.1$), $\bar{J}/J_s = 1.3$ ($T/T_D = 1$), and $\bar{J}/J_s = 1.05$ ($T/T_D = 6$). The last curve ($T/T_D = 6$) is marked
351 with an arrow to indicate that for conditions falling above this line we expect no flux
352 enhancement. The observations from Denny and Roberson (2002) are shown as dots marked
353 with the flux enhancement measured for their exposed blades. The sheltered blades fall at the
354 same positions in Fig. 7 and have comparable flux enhancement (Table 1). Note that the Denny
355 and Roberson (2002) experiments measured heat flux in air. Because ν and D are different in
356 water, altering the relationship between velocity and T_D, we adjusted the flow speed reported in
357 Denny and Roberson (2002) to represent an equivalent T_D in water. Specifically, we chose a
358 velocity $U_{\text{water,}}$ such that the ratio $T_{D\text{-air}}/T_{D\text{-water}} = (U_{\text{water}}/U_{\text{air}})^2 (D_{\text{air}}/D_{\text{water}}) (S_{c\text{-air}}/S_{c\text{-water}})^{4/3} = 1$.
359 Using the parameters given previously, $U_{\text{water}} = 0.8\ U_{\text{air.}}$ Again we see that Denny and
360 Roberson's high flow conditions produced no flux enhancement, but under the low flow
361 condition, produced flux enhancements of as much at 2.9, consistent with the surface renewal
362 model.

363 Disturbance periods that correspond to the flapping frequencies observed in this study are
364 shown with the shaded box. At low flow speeds, the observed periods overlay a region of
365 significant flux enhancement potential. For example, at $U = 0.1$ m s^{-1}, conditions for flux
366 enhancement between 1.3 and 3.5 are predicted. However, at high flow, e.g., $U > 1$ m s^{-1}, the
367 observed periods of motion fall within the region of no flux enhancement, i.e., lie above the line

368 T/T_D =6. This suggests that flapping is more beneficial to nutrient uptake at sheltered sites (low
369 flow), than at exposed sites. Although not pronounced in the current study, the ruffled
370 morphology may enhance flapping, in particular when the frequency of vortex shedding from
371 individual ruffles matches the blade's natural frequency. To the extent that ruffles enhance
372 flapping, the following conclusion is suggested. At exposed sites (high mean flow), the observed
373 range of blade flapping frequency provides little enhancement to blade flux, and the fluxes are
374 very high at these sites anyway, so there is little benefit to a ruffled morphology. In addition, the
375 ruffled morphology produces a large drag, so that this morphology provides a significant
376 disadvantage in a high flow environment (Koehl 1999). These tendencies may explain why
377 streamlined blade shapes are generally found in regions of high flow. At sheltered sites (low
378 mean flow), the renewal model suggests that measured flapping frequencies have the potential to
379 significantly enhance the flux to the blade surface, so there is benefit to a ruffled morphology. In
380 addition, in low flow drag is small for all morphologies, so that the disadvantage of a ruffled
381 morphology, in terms of drag, is not significant. These tendencies may explain why a ruffled
382 morphology is generally found in regions of low flow.
383

384 *References* –

385 Blevins, R. 1990. Flow-induced vibration. 2nd ed. Krieger Publishing.

386 Boundreau, B., and B. Jorgensen. 2001. The benthic boundary layer: Transport and
387 biogeochemistry. Oxford University Press.

388 Carslaw, H., and J. Jaeger. 1959. Conduction of heat in solids. Oxford Univ. Press.

389 Denny, M., and L. Roberson. 2002. Blade motion and nutrient flux to the kelp, *Eisenia arborea*.
390 Biol. Bull. **203**: 1-13.

391 Garcia, H. E., R. A. Locarnini, T. P. Boyer, and J. I. Antonov. 2010. World Ocean Atlas 2009,
392 volume 4: Nutrients (phosphate, nitrate, silicate). S. Levitus [ed.], NOAA Atlas NESDIS 71,
393 U.S. Government Printing Office. http://www.nodc.noaa.gov/OC5/WOA09/pr_woa09.html

394 Gerard, V., and K. Mann. 1979. Growth and production of *Laminaria longicruris* (Phaeophyta)
395 populations exposed to different intensities of water movement. J. Phycol. **15**: 33-41.

396 Haring, R., and R. Carpenter. 2007. Habitat-induced morphological variation influences
397 photosynthesis and drag on the marine macroalga *Pachydictyon coriaceum*. Mar. Biol. **151**:
398 243-255.

399 Higbie, R. 1935. The rate of absorption of a pure gas into a still liquid during short periods of
400 exposure. Trans. Am. Inst. Chem. Eng. **31**: 365 – 389.

401 Hurd, C., P. Harrison, and L. Druehl. 1996. Effect of seawater velocity on inorganic nitrogen
402 uptake by morphologically distinct forms of Macrocystis integrifolia from wave-sheltered
403 and exposed sites. Marine Bio. **126**: 205-214.

404 Hurd, C., and C. Stevens. 1997. Flow visualization around single- and multiple seaweeds with
405 various morphology. J. Phycol. **33**: 360-367.

406 Hurd, C. 2000. Water motion, marine macroalgal physiology, and production. J. Phycol. **36**:
407 453-472.
408 Koch, E. 1993. The effect of water flow on photosynthetic processes of the alga *Ulva lactuca L.*
409 Hydrobiologia **260/261**: 457-462.
410 Koch, E. 1994. Hydrodynamics, diffusion-boundary layers and photosynthesis of the seagrass
411 *Thalassia testudinum* and *Cymodocea nodosa*. Mar. Bio. **118**: 767-776.
412 Koehl, M., and R. Alberte. 1988. Flow, flapping, and photosynthesis of *Nereocystis luetkeana*: a
413 functional comparison of undulate and flat blade morphology. Mar. Biol. **99**: 435-444.
414 Koehl, M. 1999. Ecological biomechanics of benthic organisms: life history, mechanical design
415 and temporal patterns of mechanical stress. J. Exp. Biol. **202**: 3469–3476.
416 Koehl, M., W. Silk, H. Liang, and L. Mahadevan. 2008. How kelp produce blade shapes suited
417 to different flow regimes: A new wrinkle. Integr. Comp. Bio. **48**: 834-851.
418 Stevens, C., and C. Hurd. 1997. Boundary-layers around bladed aquatic macrophytes.
419 Hydrobiologia **346**: 119-128.
420 Stevens, C., C. Hurd, and P. Isachsen. 2003. Modelling of diffusion boundary-layers in subtidal
421 macroalgal canopies: response to waves and currents. Aq. Sci. **65**: 81-91.
422 Street, V., and E. B. Wylie. 1985. Fluid mechanics, 8th edition. McGraw-Hill.
423 Wheeler, W. 1980. Effect of boundary layer transport on the fixation of carbon by the giant kelp
424 *Macrocystis pyrifera*. Mar. Biol. **56**:103-110.

Table 1. Summary of measurements from Denny and Roberson (2002) and estimates of relevant time scales. Experiments were conducted in air, for which $\nu = 15 \times 10^{-6}$ m^2 s^{-1}. The thermal diffusivity is $D = 18.9 \times 10^{-6}$ m^2 s^{-1}. The Schmidt number is $Sc = 0.79$. The friction velocity was not given. The best fit between observed and predicted flux enhancement was achieved using $u_* = 0.07U$. Fluxes for the low and high speed conditions are taken from fig. 4 and 5, respectively, in Denny and Roberson (2002), and given in arbitrary units. Flux enhancement is defined as the flux with pitching normalized by the flux with no motion.

	Low speed conditions	High speed conditions
U (m s^{-1})	0.38	2.82
$u_* = 0.07\ U$ (m s^{-1})	0.027	0.20
δ_v (m) = $10\nu/u_*$	0.0056	0.00075
δ_D (m) = $\delta_v\ S_c^{-1/3}$	0.0060	0.00081
$T_D = \delta_D^2/D$ (s)	1.9	0.035
$T = (1/2)f^1$ (s)	0.85 to 3.8 s	0.85 to 3.8 s
T/T_D	0.45 to 2	24 to 108

Pitching frequency (Hz)	sheltered		exposed		sheltered		exposed	
	flux	flux enhance ment	flux	flux enhance ment	flux	flux enhance ment	flux	flux enhance ment
0 (no motion)	3.0	------	4.5	------	16	------	35	
0.13	3.3	1.1	5.1	1.1	15	0.94	34	0.97
0.20	3.8	1.3	5.8	1.3	15	0.94	38	1.1
0.39	4.9	1.6	7.1	1.6	15	0.94	33	0.94
0.59	6.8	2.3	13.1	2.9	15	0.94	35	1.0

Table 2. Summary of measurements from Koehl and Alberte (1988). Flux enhancement is defined as the flux with flapping normalized by the flux with no motion.

$U(ms^{-1})$	4.3×10^{-3}	8.5×10^{-3}
Flux with no flapping (μg C cm^{-2} h^{-1})	0.21	0.43
Flux with 1-3 Hz flapping (μg C cm^{-2} h^{-1})	0.42	0.69
Flux enhancement	2.0	1.6

Table 3. Geometric properties of *Laminaria saccharina*, *Macrocystis pyrifera*, and *Nereocystis luetkeana* blades tested in this study. R and F stand for ruffle and flat blades, respectively.

Species	Blade	Length ±0.2cm	Width ±0.1 cm	Thickness ±0.01mm	Ruffle		Winkle	
					wavelength ±0.1cm	amplitude ±0.1cm	wavelength ±0.1cm	amplitude ±0.1cm
L. saccharina	R1	41.5	8.0	0.2	2.1	0.7	1.4	0.1
	R2	16.3	4.2	0.3	2.6	0.6	na	na
	R3	45.0	8.0	0.2	2.6	0.7	na	na

					Corrugation		Spike	
					width ±0.1 cm	amplitude ±0.1cm	density ±0.1 cm^{-1}	density ±0.1 cm^{-1}
M. pyrifera	F1	46.5	9.5	0.5	4.4	1.0	1.4	2.3
	F2	43.5	8.6	0.5	4.5	1.0	1.5	2.1
	F3	46.0	9.4	0.4	4.4	0.9	1.4	2.4

					Ruffle	
					wavelength ±0.1cm	amplitude ±0.1cm
N. luetkeana	R1	97.0	6.1	0.4	1.5	0.3
	R2	118.0	4.7	0.5	2.3	0.6
	R3	101.4	5.4	0.5	2.0	0.4
	R4	124.3	5.4	0.6	2.0	0.6
	F1	121.0	4.2	0.4	na	na
	F2	61.0	4.7	0.4	na	na
	F4	30.0	4.2	0.4	na	na

Figure 1. Evolution of concentration profile adjacent to a blade. The diffusive sub-layer is stripped at $t = 0$ and evolves back to a steady profile in time $T_D = \delta_D^2/D$. The concentration (C) is normalized by the concentration at the outer edge of the diffusive sub-layer (C_o). The vertical distance (z) is normalized by the diffusive sub-layer thickness (δ_D).

Figure 2. Instantaneous (instant.) flux vs. time. In case 1 (thick line), the time between each boundary-layer disturbance (renewal period) is T_1, which is longer that the diffusive time-scale T_D. In case 2 (thin line), the time between each boundary-layer disturbance is $T_2 << T_D$. The static boundary layer flux (J_s) predicted for both cases is shown on the vertical axis. The time-average flux ($\bar{J}$) for each case is shown by a horizontal dashed line.

Figure 3. Time-averaged flux ($\bar{J}$) normalized by static sub-layer flux (J_s). T_D is the diffusive-time scale, and T is the time between periodic disturbances. Equation 5 is shown by a thick grey line. Equation 6, normalized by J_s, is shown by a thin black line. Measurements for the exposed (triangle) and the sheltered (circle) morphology taken from Denny and Roberson (2002). Flux measurements made by Koehl and Alberte (1988) shown by solid squares.

Figure 4. Geometry and Strouhal number for a corrugated plate. The vortex shedding scale (d) is half the undulation wavelength (λ). Image of a sheltered-site blade of *Nereocystis luetkeana* with pronounced ruffles from Koehl et al. 2008.

Figure 5. (a) Time record of tip position for *M. pyrifera* blade in a 22 cm s^{-1} current. Spectral analysis reveals peaks at 0.10, 0.19, and 0.41 Hz. (b) Examples of the instantaneous position of blade in a 22 cm s^{-1} current. The position along the blade (x) is expressed as a percent of total blade length (L).

Figure 6. (a) Minimum (open symbol) and maximum (solid symbol) frequency peaks detected in FFT of blade tip position for each velocity condition. (b) Amplitude of tip motion normalized by blade length plotted against velocity. Observations from Koehl and Alberte (1988) are include for ruffled (heavy diamond) and flat (heavy square) *N. luetkeana* blades that were each 1-m long. Vertical bars in both sub-plots represent one standard deviation of the distribution of values measured in a given sub-group.

Figure 7. The four lines are contours of constant flux enhancement ($\bar{J}/J_s$ = 1.05, 1.3, 3.5, 10). These contours correspond to the time-scale ratios T/T_D =*6, 1, 0.1, 0.01*, respectively. Grey shading denotes the range of disturbance periods that correspond to the blade frequencies reported in Figure 6, $T=(1/2)f^{1}$. The dots represent the data of Denny and Roberson (2002), with the velocity adjusted to account for difference in fluid media (air vs. water). The flux enhancement for the exposed morphology is shown next to each dot. Values are similar for the sheltered morphology, as shown in Table 1.

Figure 1

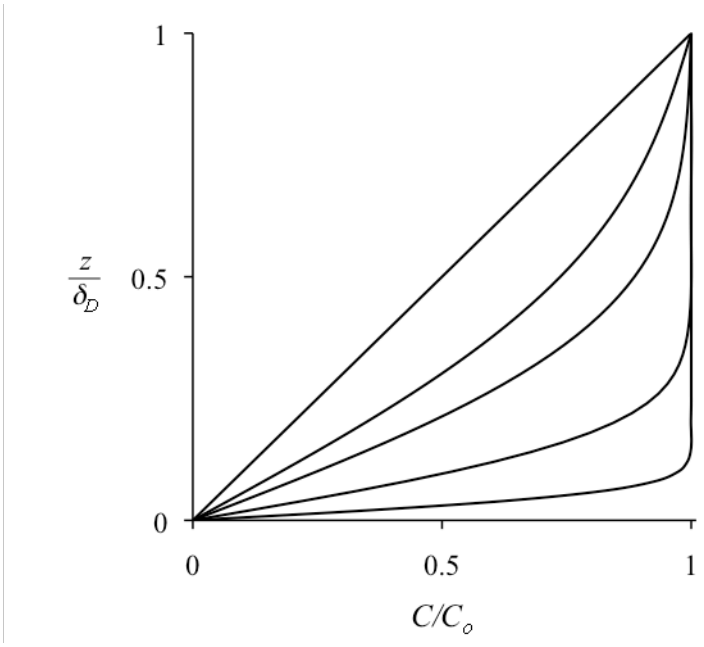

Figure 2

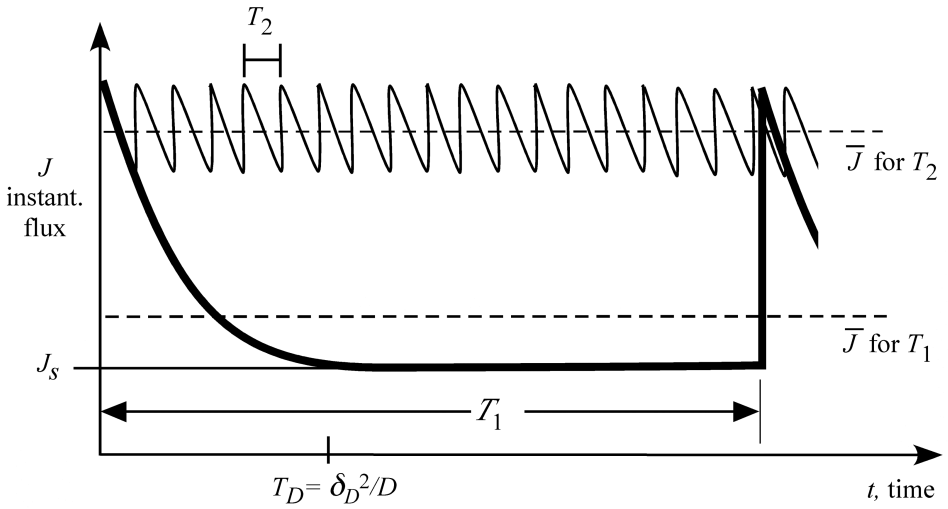
T_2
J
instant.
flux
$\overline{J}$ for T_2
$\overline{J}$ for T_1
J_s
T_1
$T_D = \delta_D^2/D$
t, time

Figure 3

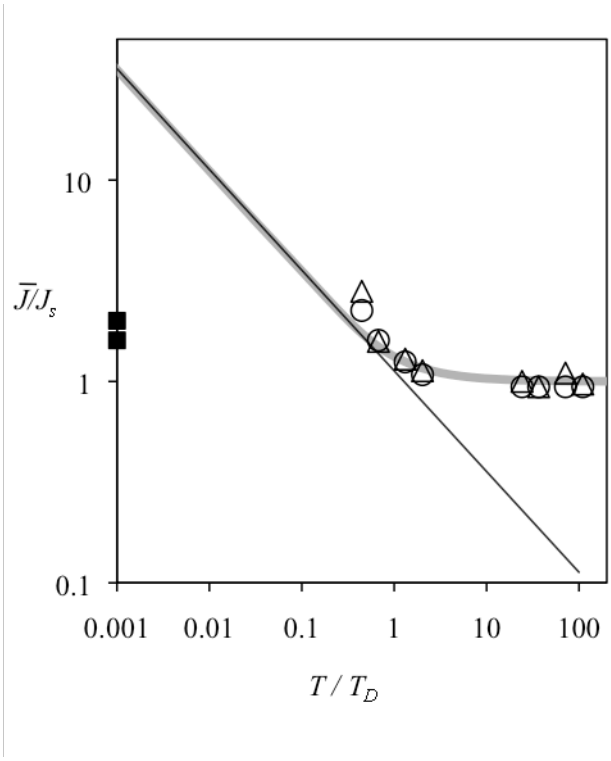

Figure 4

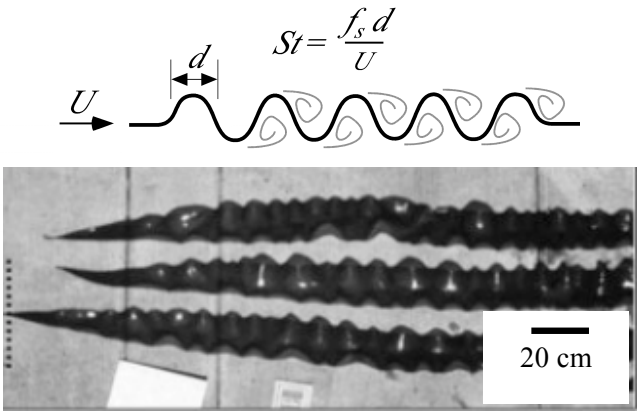

Figure 5

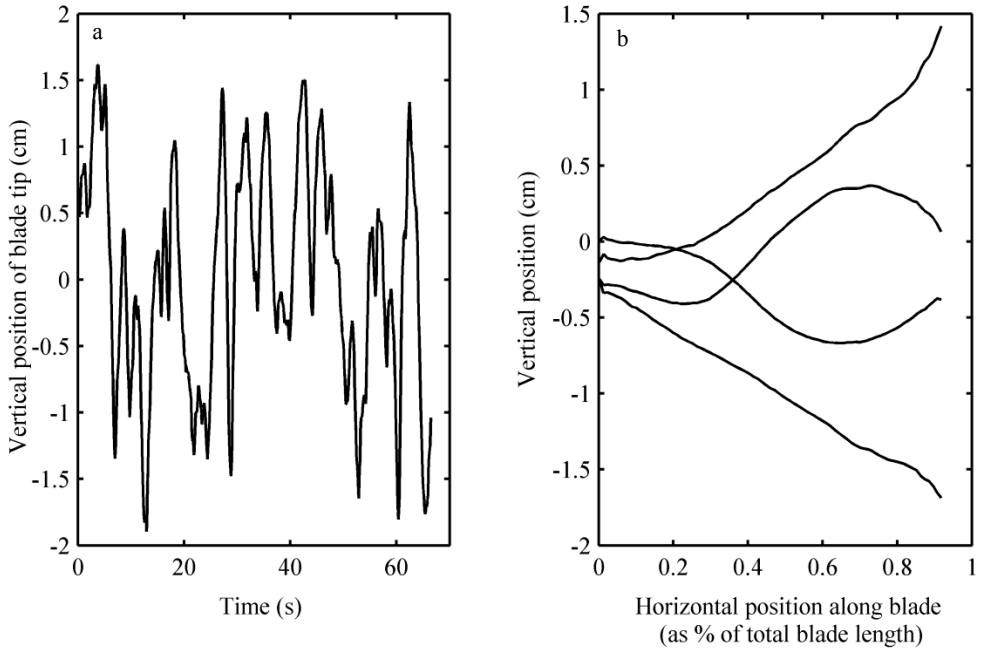
a
Vertical position of blade tip (cm)
Time (s)
b
Vertical position (cm)
Horizontal position along blade
(as % of total blade length)

Figure 6

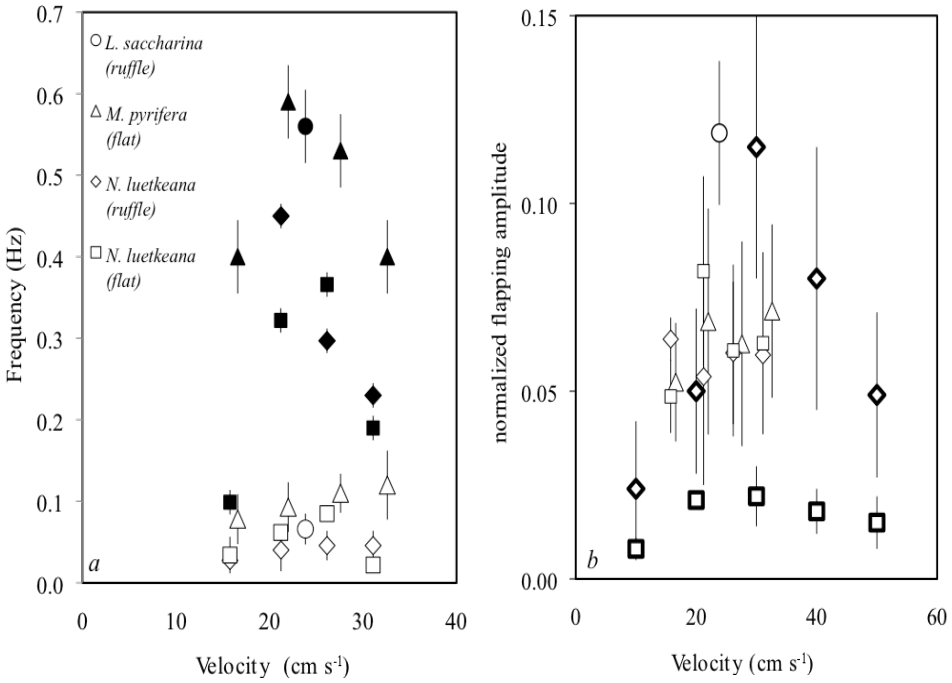
0.7
0.6
0.5
0.4
0.3
0.2
0.1
0.0
Frequency (Hz)
L. saccharina (ruffle)
M. pyrifera (flat)
N. luetkeana (ruffle)
N. luetkeana (flat)
a
0
10
20
30
40
Velocity (cm s-1)
0.15
0.10
0.05
0.00
normalized flapping amplitude
b
0
20
40
60
Velocity (cm s-1)

Figure 7.

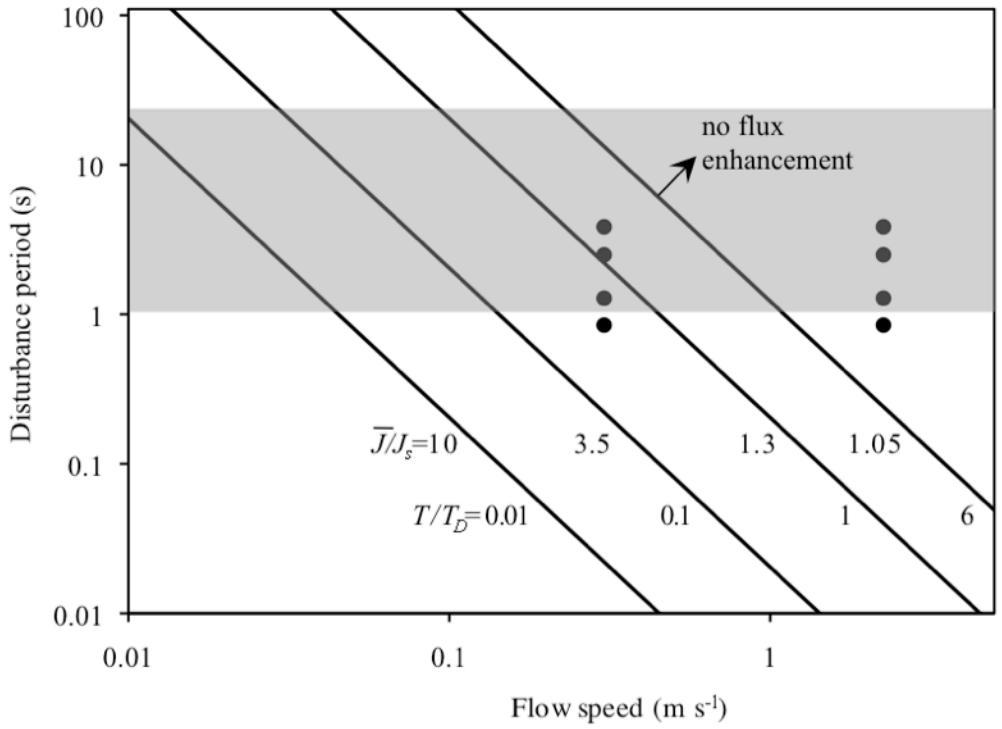
100
10
1
0.1
0.01
Disturbance period (s)
no flux
enhancement
$\overline{J}/J_s$=10
3.5
1.3
1.05
T/T_D=0.01
0.1
1
6
0.01
0.1
1
Flow speed (m s^{-1})